

Modeling Intensity-Duration-Frequency curves for the whole range of precipitation: A comparison of models

Abubakar Haruna¹, Juliette Blanchet², and Anne-Catherine Favre³

¹Université Grenoble Alpes

²Université Grenoble Alpes

³CNRS, IRD, IGE, Grenoble INP

November 24, 2022

Abstract

Intensity-Duration-Frequency curves are useful in water resources engineering for the planning and design of hydrological structures. As opposed to the common use of only extreme data to build IDF curves, here, we use all the non-zero rainfall intensities, thereby making efficient use of the available information. As a parametric model, we use the Extended Generalized Pareto Distribution (EGPD) for the non-zero intensities. We consider three commonly used approaches to build the IDF curves. The first approach is based on the scale-invariance property of rainfall, the second relies on the general IDF formulation of Koutsoyiannis et al. (1998) while the last approach is purely data-driven (Overeem et al., 2008). Using these three approaches, and some extensions around them, we build a total of 10 models for the IDF curves and then we compare them in a split-sampling cross-validation framework. We consider a total of 81 stations at 10 min resolution in Switzerland. The results reveal the model based on the data-driven approach as the best model. It is able to correctly model the observed intensities across duration while being reliable and robust. It is also able to reproduce the space and time variability of extreme rainfall across Switzerland.

Modeling Intensity-Duration-Frequency curves for the whole range of precipitation: A comparison of models

Abubakar Haruna ¹, Juliette Blanchet ², Anne-Catherine Favre ¹

¹Univ. Grenoble Alpes, Grenoble INP, CNRS, IRD, IGE, 38000 Grenoble, France

²Univ. Grenoble Alpes, CNRS, IRD, Grenoble INP, IGE, 38000 Grenoble, France

Key Points:

- We build IDF curves using all the non-zero precipitation data and model the intensities with the Extended Generalized Pareto Distribution (EGPD).
- We consider three approaches to building IDF curves: scale invariance, the general IDF formulation of Koutsoyiannis et al. (1998) and a data-driven method.
- We compare and select the best model in a cross-validation framework.

Corresponding author: Abubakar Haruna, abubakar.haruna@univ-grenoble-alpes.fr

12 Abstract

13 Intensity-Duration-Frequency curves are useful in water resources engineering for the plan-
 14 ning and design of hydrological structures. As opposed to the common use of only ex-
 15 treme data to build IDF curves, here, we use all the non-zero rainfall intensities, thereby
 16 making efficient use of the available information. As a parametric model, we use the Ex-
 17 tended Generalized Pareto Distribution (EGPD) for the non-zero intensities. We con-
 18 sider three commonly used approaches to build the IDF curves. The first approach is
 19 based on the scale-invariance property of rainfall, the second relies on the general IDF
 20 formulation of Koutsoyiannis et al. (1998) while the last approach is purely data-driven
 21 (Overeem et al., 2008). Using these three approaches, and some extensions around them,
 22 we build a total of 10 models for the IDF curves and then we compare them in a split-
 23 sampling cross-validation framework. We consider a total of 81 stations at 10 min res-
 24 olution in Switzerland. The results reveal the model based on the data-driven approach
 25 as the best model. It is able to correctly model the observed intensities across duration
 26 while being reliable and robust. It is also able to reproduce the space and time variabil-
 27 ity of extreme rainfall across Switzerland.

28 1 Introduction

29 Intensity-Duration-Frequency (IDF) curves provide the link between precipitation
 30 intensity, duration, and non-exceedance frequency (or rather the return period). It is a
 31 very common and useful tool in the area of water resources engineering. IDF curves are
 32 practically used to infer high return levels of rainfall intensities for the hydrological de-
 33 signs of structures such as sewer lines, culverts, drains, dams, dykes, etc. They are also
 34 used to calibrate/validate stochastic weather generators (Willems, 2000; Ritschel et al.,
 35 2017).

36 IDF curves are traditionally modeled by fitting a statistical model, *e.g.* a Gumbel
 37 distribution, to extreme data of each duration separately. Secondly, selected return lev-
 38 els, *e.g.* 2, 5, 10 years are obtained for each duration using the fitted distribution. And
 39 lastly, the inferred return levels are linked to duration by some empirical formulation (*e.g.*
 40 Sherman, 1931; Bernard, 1932; Chow, 1962; Carreteras, 1987; Meylan et al., 2012). Al-
 41 though common and easy to implement, there are several drawbacks to this approach.
 42 The method lacks parsimony because several parameters have to be fitted (a set for each
 43 return period). It is not robust in the sense that IDF curves are only available for spe-
 44 cific return levels, each time a new return level is needed, the process has to be repeated.
 45 Another major drawback is that uncertainty in the return levels obtained at the initial
 46 steps is not taken into account in the last step. Lastly, there can be intersections between
 47 curves of different return levels that cannot be theoretically justified.

48 To overcome the outlined limitations of the traditional parametric methods, novel
 49 approaches were considered to link the different durations together in IDF curves. In gen-
 50 eral, in spite of the approach, two choices have to be made: the specific form of the IDF
 51 curves and the parametric model for the rainfall intensities. Regarding the specific form
 52 of the IDF curves, many formulations that are based on different approaches have been
 53 proposed in the literature. Here we identify and focus on three major approaches.

54 The first approach involves the general formulation of Koutsoyiannis et al. (1998),
 55 a generalization of the various empirical formulations for modeling IDF. This formula-
 56 tion has the key advantage of being a separable function of return levels and duration.
 57 It is also consistent with both probabilistic theories and the physical constraints of scal-
 58 ing across duration. Several application of this formulation to build IDF curves can be
 59 found in the literature (*e.g.* Koutsoyiannis et al., 1998; Van de Vyver & Demarée, 2010;
 60 Blanchet et al., 2016; Sane et al., 2018; Ulrich et al., 2020; Fauer et al., 2021; Roksvåg
 61 et al., 2021).

62 The second approach is based on scale invariance. It has been shown that rainfall
63 exhibits this property within some scales (see Schertzer & Lovejoy, 1987; Gupta & Waymire,
64 1990, 1993; Over, 1995; Harris et al., 1997; Lima, 1998; Molnar & Burlando, 2008; Veneziano
65 & Lepore, 2012; Paschalis, 2013). This property provides the physical justification for
66 modeling IDF, and thus the possibility of inferring return levels of interest across scales.
67 This approach is arguably the most commonly used approach, possibly because of its rich
68 theoretical background, physical basis, and ease of application in regions with scarce avail-
69 ability of sub-daily rainfall series. IDF curves based on this approach can be found in
70 several applications (Burlando & Rosso, 1996; Menabde et al., 1999; Willems, 2000; Van de
71 Vyver & Demarée, 2010; Blanchet et al., 2016; Innocenti et al., 2017; Sane et al., 2018).

72 The last approach is termed by Vereem et al. (2008) as data-driven. The method
73 involves fitting a parametric model, for example, GEV, to data of each duration. A par-
74 ticular regression model is then fitted for each parameter as a function of duration. As
75 a consequence, the return level of any duration can be inferred from the inverse of the
76 distribution, with parameters obtained from the regression model. This approach im-
77 poses neither the assumption/existence of scaling nor the separability condition in the
78 case of the general formulation of Koutsoyiannis et al. (1998). Interestingly, both approaches
79 can be seen as data-driven approaches with particular functional relationships imposed
80 on the parameters.

81 There exists also nonparametric approaches, which rather than imposing a para-
82 metric model on the intensities, use stochastic rainfall models to estimate the IDF curves
83 (for a brief review, see Langousis & Veneziano, 2007; Veneziano et al., 2007; Tyralis &
84 Langousis, 2019). Here, we focus on the class that uses parametric models for the inten-
85 sities.

86 Coming back to the choice of parametric model for the intensities, extreme value
87 distributions are usually used. For example, Generalized Extreme Value (GEV) (e.g. Blanchet
88 et al., 2016; Innocenti et al., 2017; Van de Vyver, 2018; Sane et al., 2018; Mélése et al.,
89 2018; Ulrich et al., 2020; Jurado et al., 2020; Fauer et al., 2021), Gumbel (Yu et al., 2004;
90 Agbazo et al., 2016; Chang et al., 2016; Ghanmi et al., 2016) for annual maximum se-
91 ries or Generalized Pareto Distribution (GPD) for the peaks over thresholds (e.g. Mad-
92 sen et al., 1995; Ben-Zvi, 2009; Van de Vyver & Demarée, 2010).

93 Although the use of these distributions is justified by the practical use of IDF, which
94 is to infer high return levels for hydrological designs, there is however, a major drawback
95 resulting from the poor utilization of already scarce data, and the delicate issue of thresh-
96 old choice in the GPD case. To address these issues, Naveau et al. (2016) recently pro-
97 posed the Extended Generalized Pareto Distribution (EGPD) to model all the non-zero
98 precipitation. It has the advantage of using all the information present in the sample of
99 non-zero rainfall data and not only one value per block (like GEV distribution) or only
100 values above a given threshold (as in GPD distribution). It doesn't require the choice
101 of GPD threshold and has the advantage of being compliant with extreme value theory
102 in both the lower and upper tails. It has been used recently in many applications (e.g.
103 Evin et al., 2018; Blanchet et al., 2019; Tencaliec et al., 2020; Rivoire et al., 2021; Le Gall
104 et al., 2022; Haruna et al., 2022). However, to the best of our knowledge, it has never
105 been used for modeling IDF curves.

106 The goal of this article is to use the EGPD to build IDF curves for the non-zero
107 precipitation intensities, based on the three outlined approaches, *i.e.*, scale-invariance,
108 the general formulation of Koutsoyiannis et al. (1998) and the data-driven approach. We
109 will compare and select the best model based on a split-sampling cross-validation frame-
110 work.

111 The rest of the paper is organized as follows: Section 2 introduces the data and the
112 area under study, and Section 3 presents the EGPD, the models for the IDF curves, and

113 the evaluation framework. Section 4 presents the results and discussion and finally Sec-
 114 tion 5 draws the conclusions and gives relevant perspectives.

115 2 Data and area under study

116 The study area is Switzerland, a small country by size with an area of 41,285 km².
 117 It however presents a complex topography with elevations ranging from 191 m to 4127 m
 118 above mean sea level. Around 30% of the area is located above the elevation of 1500 m
 119 above sea level. This results in marked spatial variability both in intensity and occur-
 120 rence of precipitation.

121 Point precipitation data from a total of 81 stations, with a minimum record length
 122 of 20 years, are available for this study. They are spread across Switzerland and their
 123 location is shown in Fig. 1. Out of this total, 71 stations belong to the SwissMetNet of
 124 the Swiss Federal Office for Meteorology and Climatology (MeteoSwiss) while 10 belong
 125 to the canton of Lucerne, a partner network of MeteoSwiss. The precipitation data is
 126 measured with a tipping-bucket gauge of 0.1 mm depth resolution at a sampling reso-
 127 lution of 10 minutes. The tipping gauge is heated in order to account for snow. The sam-
 128 ple data has a variable length ranging from a minimum of 20 years to a maximum of 40 years
 129 from 1981 to 2020. The stations are located at elevations ranging from a minimum of
 203 m, an average of 952.4 m, and a maximum of 3294 m.

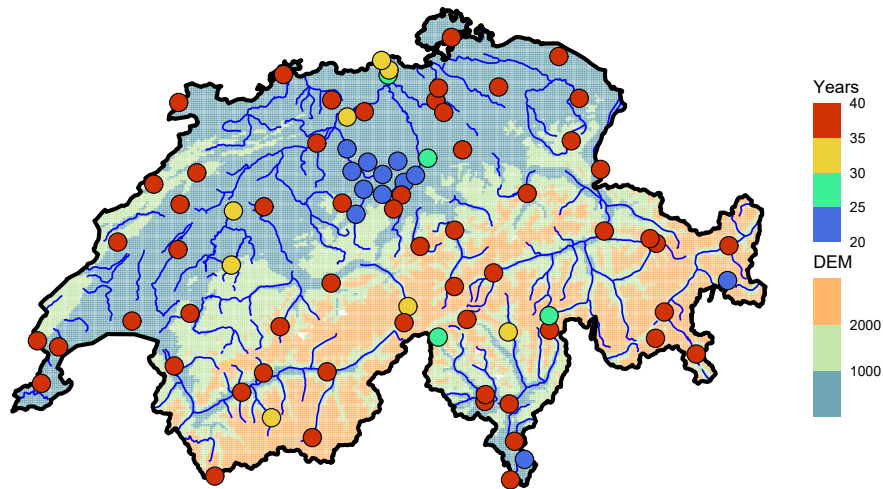


Figure 1. Map of Switzerland showing the location of the 81 stations. The color of the points indicates the length of the precipitation data in years. The background color shows the elevation above sea level in meters.

130

131 Due to the marked seasonality of precipitation in Switzerland, we divided the data
 132 into four seasons of three months each. Winter includes Dec-Jan-Feb, Spring Mar-Apr-
 133 May, Summer Jun-Jul-Aug while Autumn includes Sep-Oct-Nov. A similar seasonal ap-
 134 proach was used by Molnar and Burlando (2008); Fukutome et al. (2015); Evin et al. (2018);
 135 Haruna et al. (2022), in the study area.

3 Methodology

In this section, we start by presenting the parametric model for the non-zero precipitation intensities, then we present the various IDF models, and finally the inference strategy to estimate the parameters.

3.1 Marginal distribution of non-zero precipitation intensities

As our target is to model the IDF curves using all the non-zero precipitation intensities, we choose the EGPD of Naveau et al. (2016) as the parametric model. The model is compliant with extreme value theory in both its upper and lower tails while providing a smooth transition in-between. It gives an alternative to the light-tailed distributions such as Gamma, which underestimates extremes (Katz et al., 2002). Four parametric families of this model have been proposed by Naveau et al. (2016) to model the transition, however, the simplest of the families is parsimonious and can adequately model precipitation intensities without the need for GPD threshold selection (see Evin et al., 2018; Le Gall et al., 2022; Haruna et al., 2022, for application in the study area). We, therefore, use it in our study.

If I is a random variable representing non-zero daily precipitation intensity that is distributed according to the EGPD, then the cumulative distribution function (CDF) is given by:

$$F(i) = \mathbb{P}(I \leq i) = G \left[H_\xi \left(\frac{i}{\sigma} \right) \right], \quad (1)$$

where G is any CDF that ensures a smooth transition between the EVT compliant upper and lower tails and satisfies the conditions given in Naveau et al. (2016), and:

$$H_\xi \left(\frac{i}{\sigma} \right) = \begin{cases} 1 - (1 + \xi \frac{i}{\sigma})_+^{-1/\xi} & \text{if } \xi \neq 0 \\ 1 - \exp(-i/\sigma) & \text{if } \xi = 0 \end{cases}, \quad (2)$$

with $a_+ = \max(a, 0)$.

For the parsimonious model we use, the function G is simply defined as $G(v) = v^k$. Therefore the model is given as:

$$F(x) = \left[H_\xi \left(\frac{i}{\sigma} \right) \right]^k \quad (3)$$

The model thus has three parameters. $k > 0$ controls the lower tail, $\xi \geq 0$ controls the upper tail, and $\sigma > 0$ is the scale parameter.

3.2 IDF models

We define the random variable I_d as the average non-zero precipitation intensity over the duration d . It is described by the CDF, $F_d(i)$, such that $F_d(i) = \mathbb{P}(I_d < i)$. The exceedance frequency is defined as $p_d(i) = 1 - F_d(i)$. The return period of any non-zero intensity i , as a function of p_d is given by $T(I_d \geq i) = \frac{1}{p_d \times \delta_d}$, with δ_d the average number of non-zero precipitation intensities per year. Conversely, the T -year return level over duration d , $i(T, d)$, is defined as the $(1 - \frac{1}{T \times \delta_d})$ quantile of F_d .

Accordingly, IDF is a mathematical function $(T, d) \mapsto i(T, d)$ that relates non-zero rainfall intensity i with its duration d , and the frequency of exceedance p_d (or rather the return level T). In this article, the CDF of I_d , $F_d(i)$ is defined by the EGPD presented in Section 3.1. All the different formulations considered here simply differ by how they define this mathematical relationship between i , T and d , while taking $F_d(i)$ as an EGPD model.

In the following subsections, we present the different IDF-EGPD models based on the three outlined approaches, *i.e.*, scale-invariance, the general formulation of Koutsoyiannis

176 et al. (1998), and data-driven approaches. For sake of simplicity, we drop the "EGPD"
 177 term and simply refer to the IDF models as $IDF_{modelname}$, where the subscript "*mod-*
 178 *ename*" refers to the approach used to build the model.

179 For all the models, the IDF curves, corresponding to the $(1 - \frac{1}{T \times \delta_d})$ quantile of
 180 the EGPD is defined in Eq. 4. The choice of the model determines whether each of the
 181 three parameters; κ , σ , and ξ depends on d or not, and the form of the relationship.

$$i(T, d) = \frac{\sigma_d}{\xi_d} \left\{ \left(1 - \left[1 - \frac{1}{T \times \delta_d} \right]^{\frac{1}{\kappa_d}} \right)^{-\xi_d} - 1 \right\} \quad (4)$$

182 We consider thirteen durations, *i.e.*, $d = 30$ min, 40 min, 1, 2, 3, 6, 10, 12, 16, 18,
 183 24, 48 and 72 hours. We use a fixed window to aggregate the data from the gauge res-
 184 olution of 10 mins, to the various durations. For instance, the 24hr intensities correspond
 185 to amounts accumulated from 00h00 to 24h00 of every day, divided by 24.

186 3.2.1 Scaling IDF

187 Scale invariance in the strict sense of Gupta and Waymire (1990) refers to the prop-
 188 erty where the probability distribution of I_d can be inferred from the distribution of I_{d_0}
 189 at the reference duration d_0 through:

$$I_d \stackrel{dist}{=} C_\lambda I_{d_0}, \quad (5)$$

190 where the parameter C_λ determines the type of scaling; simple-scaling or multi-scaling.

191 A weaker assumption, the so-called "wide sense scaling" (Gupta & Waymire, 1990),
 192 is when the scaling is in the moments according to:

$$\mathbb{E}[I_d^q] = \left(\frac{d}{d_0} \right)^{-k(q)} \mathbb{E}[I_{d_0}^q], \quad (6)$$

193 where q is the order of the moment, $k(q)$ is called the moment scaling function, d_0 is the
 194 reference duration. Moment scaling analysis as described by Gupta and Waymire (1990)
 195 is used to determine the type of scaling.

196 Strict sense simple-scaling occurs when the scale ratio C_λ in Eq. 5 is a scalar that
 197 depends only on the ratio of the scales as expressed in Eq. 7.

$$I_d \stackrel{dist}{=} \left(\frac{d}{d_0} \right)^{-H} I_{d_0} \quad (7)$$

198 Wide sense simple-scaling is when the moment scaling function in Eq. 6 is linear
 199 in q , *i.e.* $k(q) = Hq$, as expressed in Eq. 8.

$$\mathbb{E}[I_d^q] = \left(\frac{d}{d_0} \right)^{-Hq} \mathbb{E}[I_{d_0}^q] \quad (8)$$

200 It can be shown that, under the strict sense simple-scaling, only one parameter of
 201 the EGPD is scaling, which is σ , whereas κ and ξ are independent of duration. For the
 202 rest of the paper, we drop the term "strict-sense", and simply use "simple-scaling" for
 203 convenience.

204 The simple-scaling EGPD model, IDF_{ss} , is defined such that: $\kappa_d = \kappa_{d_0}$, $\xi_d =$
 205 ξ_{d_0} , and σ_d is a power law given as:

$$\sigma_d = \left(\frac{d}{d_0} \right)^{-H} \sigma_{d_0} \quad (9)$$

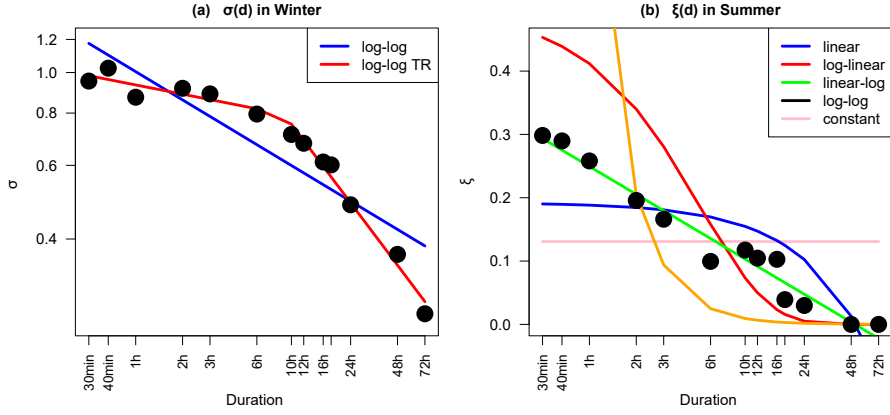


Figure 2. Illustration of **a)** Break in scaling of the σ parameter in winter at a station, Robbia in Graubünden. The points colored in black are the estimated σ for each duration separately. **b)** Dependence of ξ on duration in summer at a station in Zurich. The black colored points are the estimated ξ for each duration separately. The lines are the fitted linear models. The pink line is the mean of the estimated ξ .

206 An important issue is the existence of multiple scaling regimes in precipitation. This
 207 means that different scaling behaviors (scaling exponents) exist for different ranges of
 208 duration. IDF then have to be modeled considering the existence of this change in scal-
 209 ing (e.g. Yu et al., 2004; Bougadis & Adamowski, 2006; Courty et al., 2019). An illus-
 210 tration of this behavior is given in Fig. 2a for the σ parameter in winter at a station,
 211 Robbia in Graubünden. Here, a single power law (log-log given in Eq. 9) in blue is not
 212 enough to explain the scaling. The two regime model (log-log TR in Eq. 10) in red is
 213 necessary.

214 To account for this break in the scaling relationship, we define the two-regime simple-
 215 scaling EGPD IDF model, IDF_{ss-TR} as:

$$\sigma_d = \begin{cases} \left(\frac{d}{d_0} \right)^{-H_1} \sigma_{d_0} & \text{if } d \leq K, \\ \left(\frac{d}{d_0} \right)^{-H_2} \sigma_{d_0} \times K^{H_2-H_1} & \text{if } d > K, \end{cases} \quad (10)$$

216 where K is the duration of the scaling break, and σ is continuous in $d = K$. The
 217 other parameters, H_1 and H_2 are the scaling exponents of the first and second regimes.
 218 The other two parameters, κ , and ξ remain independent of durations. Hence for this model,
 219 a total of six parameters have to be estimated, *i.e.*, κ_{d_0} , σ_{d_0} , ξ_{d_0} , H_1 , H_2 and K .

220 Lastly, although the simple-scaling EGPD model imposes a constraint on the de-
 221 pendence of ξ with d , *i.e.*, $\xi_d = \xi_{d_0}$, we however notice some of the stations to show ap-
 222 parent dependence of ξ with respect to d . To account for this, we impose a functional
 223 relationship of ξ with respect to duration through a linear-log form as expressed in Eq.
 224 11. Fig. 2b gives an example of the dependence of ξ on duration at a station in Zurich,
 225 and how the linear-log model fits correctly the points.

$$\xi_d = a_\xi + b_\xi \log(d) \quad (11)$$

Where a_ξ and b_ξ are the intercepts and slopes respectively. This leads to two additional IDF models, with $\xi = f(d)$, namely:

- $\text{IDF}_{ss-\xi(d)}$: an extension of the basic simple-scaling model IDF_{ss} , to allow ξ to depend on d according to Eq. 11.
- $\text{IDF}_{ss-TR-\xi(d)}$: an extension of the two-regime simple-scaling model IDF_{ss-TR} , to allow ξ to depend on d according to Eq. 11.

3.2.2 General IDF formulation

Koutsoyiannis et al. (1998) proposed a general formulation for the different traditional formulations of the IDF curves in the literature. He showed that all of them can be simplified into the form:

$$i(T, d) = \frac{a(T)}{b(d)} \quad (12)$$

where $b(d) = (d + \theta)^H$. The parameter θ is the duration offset, and H is the duration exponent. Both θ and H are non-negative constants. $a(T)$ is the $(1 - \frac{1}{T})$ quantile of the re-scaled intensities $I_d b(d)$. $a(T)$ is independent of d and completely determined by the statistical model considered for I_d , in our case, the EGPD.

This formulation has the key advantage of being a separable function of return levels $a(T)$, and duration $b(d)$ that is consistent with both probabilistic theories and the physical constraints of scaling across duration. Menabde et al. (1999) showed that this formulation is the same as the scale-invariant model θ is set to zero.

When applied to the EGPD, IDF_{koust} is defined such that: $\kappa_d = \kappa_{d_0}$ $\sigma_d = \left(\frac{d+\theta}{d_0+\theta}\right)^{-H} \sigma_{d_0}$ $\xi_d = \xi_{d_0}$. Five parameters, κ , σ , ξ , θ and H have to be inferred.

Following the same arguments discussed in Section 3.2.1 regarding the existence of a break in the scaling relationship, and the dependence of ξ with d , we propose three extensions to this model:

- $\text{IDF}_{koust-TR}$: Allowing for a break in the scaling regime. This model is defined as:

$$\sigma_d = \begin{cases} \left(\frac{d+\theta}{d_0+\theta}\right)^{-H_1} \sigma_{d_0} & \text{if } d \leq K \\ \left(\frac{d}{d_0}\right)^{-H_2} \sigma_{d_0} \times K^{H_2-H_1} & \text{if } d > K \end{cases} \quad (13)$$

where κ and ξ are independent of duration.

- $\text{IDF}_{koust-\xi(d)}$: an extension of the basic model IDF_{koust} , to allow ξ to depend on d according to Eq. 11.
- $\text{IDF}_{koust-TR-\xi(d)}$: an extension of the two-regime model $\text{IDF}_{koust-TR}$, to allow ξ to depend on d according to Eq. 11.

3.2.3 Data-Driven IDF

The scaling theory and the specific form of Eq. 12 impose particular functions for the relation between the scale parameter, σ of the EGPD with respect to duration, d . However, in the case of the data-driven models, the expression of the relationship for each of the three EGPD parameters is entirely determined by the data itself. To guide our choice of the appropriate functional relationship, we inspected how each locally estimated parameter varies with duration. Fig. 2 gives an example for the σ and ξ parameters at two stations. We finally settled on the following functions to model the three parameters with respect to duration:

$$\kappa_d = \begin{cases} \exp [a_\kappa + b_{1,\kappa} \log (d)] & \text{if } d \leq K_\kappa \\ \exp [a_\kappa + b_{2,\kappa} \log (d) + (b_{1,\kappa} - b_{2,\kappa}) \log (K_\kappa)] & \text{if } d > K_\kappa \end{cases} \quad (14)$$

$$\sigma_d = \begin{cases} \exp [a_\sigma + b_{1,\sigma} \log (d)] & \text{if } d \leq K_\sigma \\ \exp [a_\sigma + b_{2,\sigma} \log (d) + (b_{1,\sigma} - b_{2,\sigma}) \log (K_\sigma)] & \text{if } d > K_\sigma \end{cases} \quad (15)$$

264 For the first two parameters, κ and σ , the function is a continuous two linear piece-
 265 wise model in log space. K_* is the duration of the breakpoint (σ continuous for $d = K$).
 266 a_* , $b_{1,*}$, $b_{2,*}$ are the intercepts and slopes of the first and second lines respectively. In the
 267 case of xi , the function os given in Eq. 11.

268 Note that, by keeping κ and σ independent of duration, and using either $\sigma_d = \left(\frac{d}{d_0}\right)^{-H} \sigma_{d_0}$
 269 or $\sigma_d = \left(\frac{d+\theta}{d_0+\theta}\right)^{-H} \sigma_{d_0}$, the simple-scaling or the general formulations of Koutsoyiannis
 270 et al. (1998) presented in Section 3.2.1 and 3.2.2 respectively can be obtained from this
 271 data-driven approach.

272 We consider two IDF models in this class, both impose the same type of functional
 273 relationships (Eq. 14, 15, 11), but simply differ in the way the regression parameters are
 274 estimated. For the first model, we follow a two-step approach (as implemented by Overeem
 275 et al., 2008). First, we fit, for a given station, the EGPD on the data of each duration
 276 separately. Second, we fit for each fitted parameter, the chosen regression model as a func-
 277 tion of duration. We call this model IDF_{DDlocal}.

278 The second model involves a one-step global fitting procedure. We pool all the data
 279 from the different durations to estimate the best EGPD with parameters from Eq. 14
 280 to 11), the duration being the covariate. We call this model IDF_{DDglobal}.

281 Note again that both models have the same number of free parameters, *i.e.* 10, but
 282 differ in the inference strategy.

283 The different models compared in this study are summarized in Table 1.

Table 1. Summary of the IDF models that are compared in this study.

Model	No. of Parameters	Name of Approach	Ref. Section
1 IDF _{ss}	4	Simple-scaling	3.2.1
2 IDF _{ss-TR}	6	Simple-scaling	3.2.1
3 IDF _{ss-ξ(d)}	5	Extension of Simple-scaling	3.2.1
4 IDF _{ss-TR-ξ(d)}	7	Extension of Simple-scaling	3.2.1
5 IDF _{kouts}	5	Koutsoyiannis et al. (1998)	3.2.2
6 IDF _{kouts-TR}	7	Extension of Koutsoyiannis et al. (1998)	3.2.2
7 IDF _{koust-ξ(d)}	6	Extension of Koutsoyiannis et al. (1998)	3.2.2
8 IDF _{koust-TR-ξ(d)}	8	Extension of Koutsoyiannis et al. (1998)	3.2.2
9 IDF _{DDlocal}	10	Data-driven	3.2.3
10 IDF _{DDglobal}	10	Data-driven	3.2.3

284 3.3 Inference

285 For the models of Koutsoyiannis et al. (1998), the authors have proposed two dif-
 286 ferent estimation strategies; the so-called ‘robust estimation’, and the ‘one-step least square
 287 method’. The robust estimation is a two-step procedure that involves the estimation of
 288 the parameters of $b(d)$, and then those of $a(T)$ (see Eq. 12), through the minimization
 289 of the Kruskal-Wallis statistic. The one-step least square method involves the joint es-
 290 timation of all the parameters of Eq. 12 that minimizes the squared error of the observed

291 and modeled quantiles from the IDF model. In the case of the simple-scaling models,
 292 a two-step procedure has been used (see Nhat et al., 2008; Panthou et al., 2014; Inno-
 293 centi et al., 2017) where the scaling exponent in Eq. 7 is first obtained through moment
 294 scaling analysis, then all re-scaled intensities from all the durations are used to fit the
 295 IDF model.

296 In our case, however, we follow a global maximum likelihood estimation for all the
 297 models, as done by Blanchet et al. (2016). This involves pooling, for each station, all the
 298 data from the thirteen durations to estimate the model parameters. The duration d is
 299 used as a covariate. We note here that by pooling all the data, the dependence between
 300 the time steps and durations is neglected.

301 The log-likelihood (l) that is maximized here (given in Eq. 16) takes left censoring
 302 into account. The importance of using left censoring in fitting rainfall data by maximum
 303 likelihood has been pointed out by Naveau et al. (2016), and he showed that better
 304 performance is obtained by taking it into account.

$$l_{EGPD}(\kappa_d, \sigma_d, \xi_d) = l_{censored}(\kappa_d, \sigma_d, \xi_d) + l_{uncensored}(\kappa_d, \sigma_d, \xi_d), \quad (16)$$

305 where $l_{censored}$ and $l_{uncensored}$ are the contributions of the censored and uncen-
 306 sored data, given in Eq. 17 and 18 respectively, as

$$l_{censored}(\kappa_d, \sigma_d, \xi_d) = \sum_d \sum_{j:i_d < c_d} \kappa \log \left[1 - \left(1 + \frac{\xi_d c_d}{\sigma_d} \right)^{-\frac{1}{\xi_d}} \right], \quad (17)$$

$$l_{uncensored}(\kappa_d, \sigma_d, \xi_d) = \sum_d \sum_{j:i_d \geq c_d} \log \kappa_d - \sum_d \sum_{j:i_d \geq c_d} \log \sigma_d - \sum_d \sum_{j:i_d \geq c_d} \left[1 + \frac{\xi_d i_{d,j}}{\sigma_d} \right]^{[1+\frac{1}{\xi_d}]} + \sum_d \sum_{j:i_d \geq c_d} \left[1 - \left(\left(1 + \frac{\xi_d i_{d,j}}{\sigma_d} \right)^{-\frac{1}{\xi_d}} \right) \right]^{[\kappa_d-1]}, \quad (18)$$

307 where c_d is the left censoring threshold applied to the data of duration d and the
 308 summation is done over the 13 durations. Many authors have taken this into account
 309 but they usually take a uniform threshold value for all the stations (e.g. Tencaliec et al.
 310 (2020) used 2 mm for daily rainfall). Here we didn't find the use of a common thresh-
 311 old over the 81 stations sufficient. We had to select, for each station and duration, the
 312 lower threshold c that minimizes the Normalized Root Mean Square Error (NRMSE) of
 313 Eq. 19 in Section 3.4.

314 In both Eq. 17 and 18, the choice of the IDF model specifies the function linking
 315 the EGPD parameters to duration. For instance, in the case of the simple-scaling , IDF_{DD_{ss}},
 316 $\kappa_d = \kappa_{d_0} \quad \sigma_d = \left(\frac{d}{d_0} \right)^{-H} \sigma_{d_0} \quad \xi_d = \xi_{d_0}$.

317 For the specific case where two linear models are fitted (see Eq. 10, 13, 14, 15, 11),
 318 we start by estimating the break-point, K , using the functions in the **segmented**  pack-
 319 age (Muggeo et al., 2008). The package implements the algorithm of Muggeo (2003) which,
 320 given the initial value of the break-point, estimates simultaneously the optimal break-
 321 point and the other parameters of the segmented linear model. The estimation is done
 322 through computational iteration of a reparameterized form of the standard segmented
 323 regression (see Muggeo, 2003, for details). We then plug the estimated value in the like-
 324 hood functions to estimate the parameters.

Finally, in the case of the IDF_{DD_{local}}, the parameters in Eq. 14 and 15 are estimated by segmented regression (described in the preceding paragraph), while those of Eq. 11 by least-squares.

3.4 Evaluation framework

We evaluate the performance of the models in two aspects. First, in calibration, that is how well a given model predicts the data that was used in training it. Secondly, we evaluate their predictive performance in a cross-validation framework.

3.4.1 Calibration

To evaluate the performance of the models in calibration, we compute the NRMS. The normalization, which here is done by the mean, allows the comparison of intensities of different duration across different stations.

For each station s , and duration d , we compute the NRMSE over the non-zero precipitation intensities as:

$$\text{NRMSE}_s(d) = \frac{\left\{ \frac{1}{n_s(d)} \sum_{j=1}^{n_s(d)} (r_{s,T_j}(d) - \hat{r}_{s,T_j}(d))^2 \right\}^{1/2}}{r_s(d)} \quad (19)$$

where $\text{NRMSE}_s(d)$ denotes the score computed at station s , and duration d , $n_s(d)$ is the number of non-zero precipitation intensities for duration d , $r_{s,T_j}(d)$ is the empirical quantile with return period T_j , $\hat{r}_{s,T_j}(d)$ is the corresponding T_j -year return level estimated from the fitted model. The denominator is the average rainfall at site s and duration d , given as $\frac{1}{n_s(d)} \sum_{j=1}^{n_s(d)} r_{s,T_j}(d)$. The best model according to this criteria is the one with the lowest $\text{NRMSE}_s(d)$.

3.4.2 Cross-validation

We follow a split sampling procedure in a cross-validation framework. For each station s , we divide the 10 min precipitation intensities into two equal sub-samples of the same length but on different years that are randomly chosen. We then aggregate the data into intensities of various duration, $d = 30$ min, 40 min, 1,2, 3, 6, 10, 12, 16, 18, 24, 48, 72 hours. Then we fit each of the 10 IDF models.

We then evaluate the performance of the models fitted on sub-sample 1 on the observations in sub-sample 2 and *vice versa*, by computing the relevant cross-validation criteria. We repeat this procedure 10 times.

In the following, we present three different criteria we use to evaluate the models. These criteria have been used in several studies to evaluate and compare competing models, (see Garavaglia et al., 2011; Renard et al., 2013; Blanchet et al., 2015; Evin et al., 2016; Haruna et al., 2022).

- The Robustness criteria, SPAN, measures the stability of the estimate of a high return level when the training data is changed. It is computed as:

$$\text{SPAN}_{s,T}(d) = \frac{2 \left| \hat{r}_{s,T}^{(1)}(d) - \hat{r}_{s,T}^{(2)}(d) \right|}{\left(\hat{r}_{s,T}^{(1)}(d) + \hat{r}_{s,T}^{(2)}(d) \right)} \quad (20)$$

where $\hat{r}_{s,T}^{(1)}(d)$ and $\hat{r}_{s,T}^{(2)}(d)$ are the T -year return levels estimated from sub-sample 1 and 2 respectively at station s and duration d .

361 For each duration d , a regional score over all the N stations ($N = 81$) is computed
 362 as $\text{SPAN}_{\text{reg},T}(d) = 1 - \frac{1}{N} \sum_{s=1}^N \text{SPAN}_{s,T}(d)$ and a perfect model in terms of
 363 robustness according to this criteria should have $\text{SPAN}_{\text{reg},T}(d) = 1$.

- 364 • The reliability of the model fitted on sub-sample 1 in predicting the maxima in
 365 sub-sample 2 and *vice versa* is measured by the FF criteria:

$$\text{FF}_s^{(12)}(d) = \left[\hat{F}_s^{(1)}(d) \left(\max_s^{(2)}(d) \right) \right]^{n_s^{(2)}(d)} \quad (21)$$

366 where $\text{FF}_s^{(12)}(d)$ is the cross-validation criteria computed at station s , and dura-
 367 tion d , by predicting the probability of the maximum value in sub-sample 2, of sam-
 368 ple size $n_s^{(2)}(d)$ using the model $\hat{F}_s^{(1)}(d)$ fitted on the sub-sample 1. $\text{FF}_s^{(21)}(d)$ is
 369 computed symmetrically.

370 For a given duration, Renard et al. (2013) and Blanchet et al. (2015) showed that
 371 each $\text{FF}_s^{(12)}(d)$ at a station should be a realization of a uniform distribution. So
 372 the difference in the area, *diff* between a theoretical uniform distribution and that
 373 of the N set of $\text{FF}_s^{(12)}(d)$ (computed over the N stations), should be close to zero.
 374 $\text{FF}_{\text{reg}}(d)$ at the regional scale, given as $1 - \text{diff}$, should therefore take a value
 375 of 1 for a reliable model; the lower the value the less reliable the model is.

- 376 • The reliability/accuracy of the model in predicting the entire observations in cross-
 377 validation is measured by the NRMSE_CV.

$$\text{NRMSE_CV}_s^{(12)}(d) = \frac{\left\{ \frac{1}{n_s^{(2)}(d)} \sum_{j=1}^{n_s^{(2)}(d)} \left(r_{s,T_j}^{(2)}(d) - \hat{r}_{s,T_j}^{(1)}(d) \right)^2 \right\}^{1/2}}{\overline{r_s^{(2)}(d)}} \quad (22)$$

378 where $\text{NRMSE_CV}_s^{(12)}(d)$ is the score computed at station s , and duration d , $n_s^{(2)}(d)$
 379 is the sample size, $r_{s,T_j}^{(2)}(d)$ is the empirical quantile with return period T_j in sub-
 380 sample 2, $\hat{r}_{s,T_j}^{(1)}(d)$ is the corresponding T_j return level estimated from $\hat{F}_s^{(1)}(d)$. The
 381 denominator is the average daily rainfall in sub-sample 2 at site s given as
 382 $\frac{1}{n_s^{(2)}(d)} \sum_{j=1}^{n_s^{(2)}(d)} r_{s,T_j}^{(2)}(d)$.

383 Finally, for each duration d , the regional score computed over the N stations is
 384 given as: $\text{NRMSE_CV}_{\text{reg}}^{(12)}(d) = 1 - \frac{1}{N} \sum_{s=1}^N \text{NRMSE_CV}_s^{(12)}(d)$.

385 $\text{NRMSE_CV}_{\text{reg}}^{(21)}(d)$ is computed in similar way. $\text{NRMSE_CV}_{\text{reg}} = 1$ means a per-
 386 fect model, and the closer the value is to 1, the more accurate the model is.

387 4 Results and discussion

388 We present the results in the following order: first we investigate the appropriate-
 389 ness of the EGPD to fit the data of each duration. Then we present the results of the
 390 comparison of the IDF models in calibration, and then in cross-validation. Finally, we
 391 show some IDF curves modeled with the best IDF.

392 4.1 Assessment of EGPD goodness of fit

393 The first issue is to investigate whether EGPD is an appropriate model for the pre-
 394 cipitation data at hand. To check this, we fitted the model at each station and for each
 395 duration, independently. We call this EGPD model fitted on each data separately as the
 396 "base" model. We then assess the quality of the resulting fits by computing the NRMSE
 397 given in Eq. 19. The seasonal boxplots of the score for each duration are shown in Fig.
 398 3. The higher the score, the better the model.

399 In spring and summer, the quality of the fit is less good for durations lower than
 400 2 hours. In winter, on the other hand, the fit is less good for $d = 48$ and 72 hours. Over-

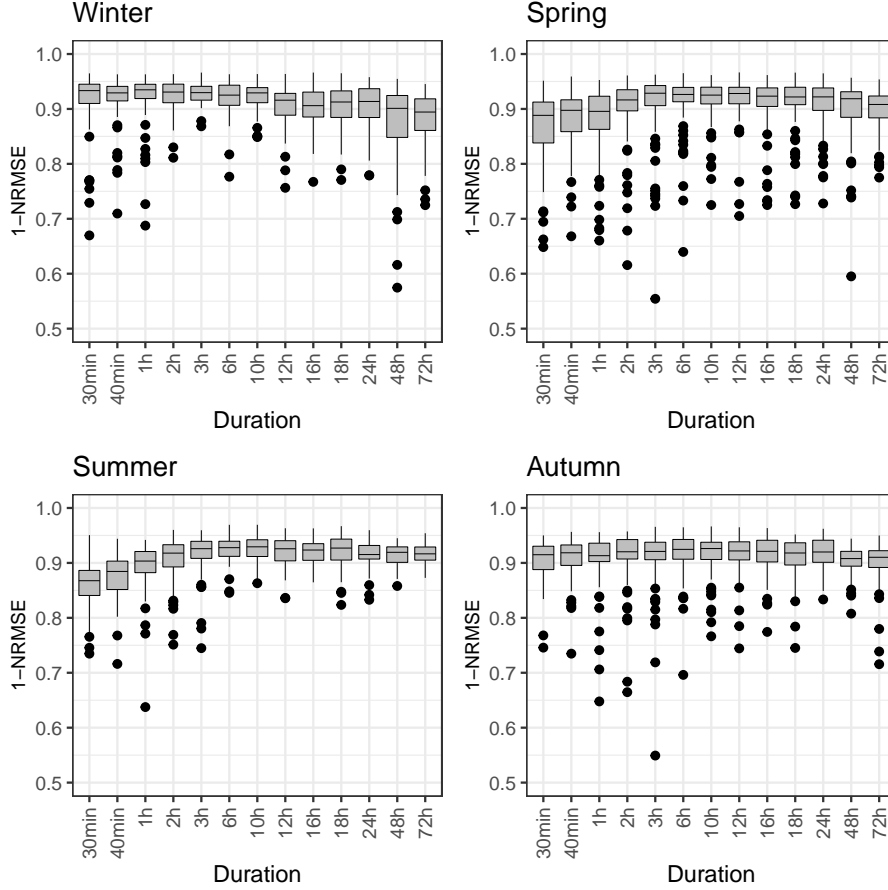


Figure 3. Boxplots of $1 - \text{NRMSE}_s(d)$ versus duration for the base EGPD model, *i.e.*, fitted on data of each duration separately. Each boxplot contains 81 points, with each point corresponding to one station.

401 all, more than 74% of the scores fall above 0.9 and 96% above 0.8. We, therefore, con-
 402 sider the EGPD to be a reasonable model for the data.

403 The fitted shape parameter ξ with respect to duration is shown on Fig. 4. Each
 404 boxplot contains 81 values, one for each station. We can strong dependence this param-
 405 eter on duration, especially in summer. For this season, while 75% of the stations have
 406 a $\xi > 0.17$ for $d = 1\text{hr}$, only 25% have $\xi > 0.06$ at $d = 24\text{hr}$. In winter, however, the
 407 dependence is not very strong, as judged by the large variability of the boxplots.

408 **4.2 Comparison of models**

409 Results of the model comparison are presented under two frameworks, first in cal-
 410 ibration, and then secondly in cross-validation based on split sampling.

411 **4.2.1 Evaluation in calibration**

412 Figure 5 presents the seasonal boxplots of the 1-NRMSE for the 10 IDF models and
 413 the base model. Each of the boxplot contains 1053 points, summarizing the score over
 414 81 stations and 13 durations. In the case of the base model (in yellow), the scores are
 415 the same as those in Fig. 3, but here we merge the scores for all the durations together.

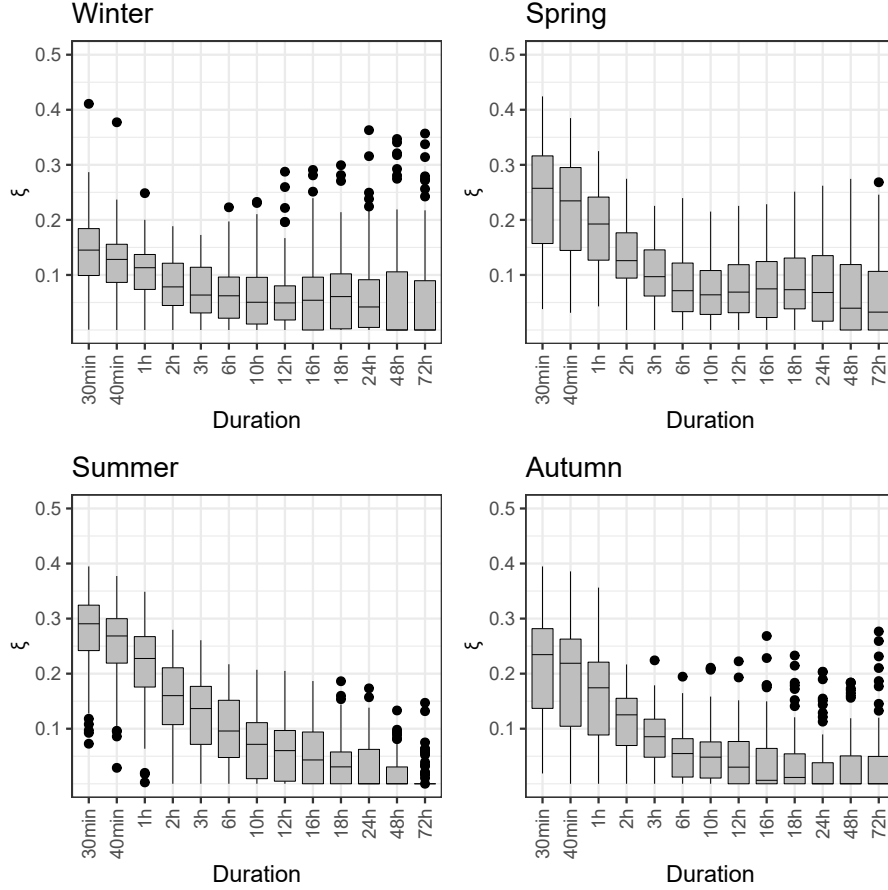


Figure 4. Boxplots of the fitted ξ versus duration obtained with the base model. Each boxplot contains 81 points, with each point corresponding to one station. The closer to 1, the better the model.

416 For all seasons, the two data-driven IDF models, $IDF_{DD_{local}}$ and $IDF_{DD_{global}}$ al-
 417 ways show the best performance compared to the others. When looking at the two, the
 418 $IDF_{DD_{global}}$ generally outperforms the $IDF_{DD_{local}}$. This means that the global fitting
 419 of the model improves the estimation performance compared to the simple interpolation
 420 of the locally estimated parameters.

421 Comparing the IDF_{ss} and the IDF_{kouts} (white *vs* red boxplots), the results show
 422 that for all seasons, the IDF_{kouts} has a better performance compared to the IDF_{ss} . Re-
 423 call that the two models differ by the additional parameter θ in the former to account
 424 for curvature for short durations.

425 Allowing for $\xi = f(d)$ increased the performance of the models mainly in sum-
 426 mer, where all the models without this addition showed very poor performance. For the
 427 other seasons, the gain in performance is not as pronounced.

428 Lastly, the models allowing for scaling break (those with subscript $_{TR}$), show im-
 429 proved performance compared to those with the single regime for all the seasons, except
 430 summer (*e.g.* IDF_{ss} vs $IDF_{ss_{TR}}$, *i.e.* the white and violet boxplots).

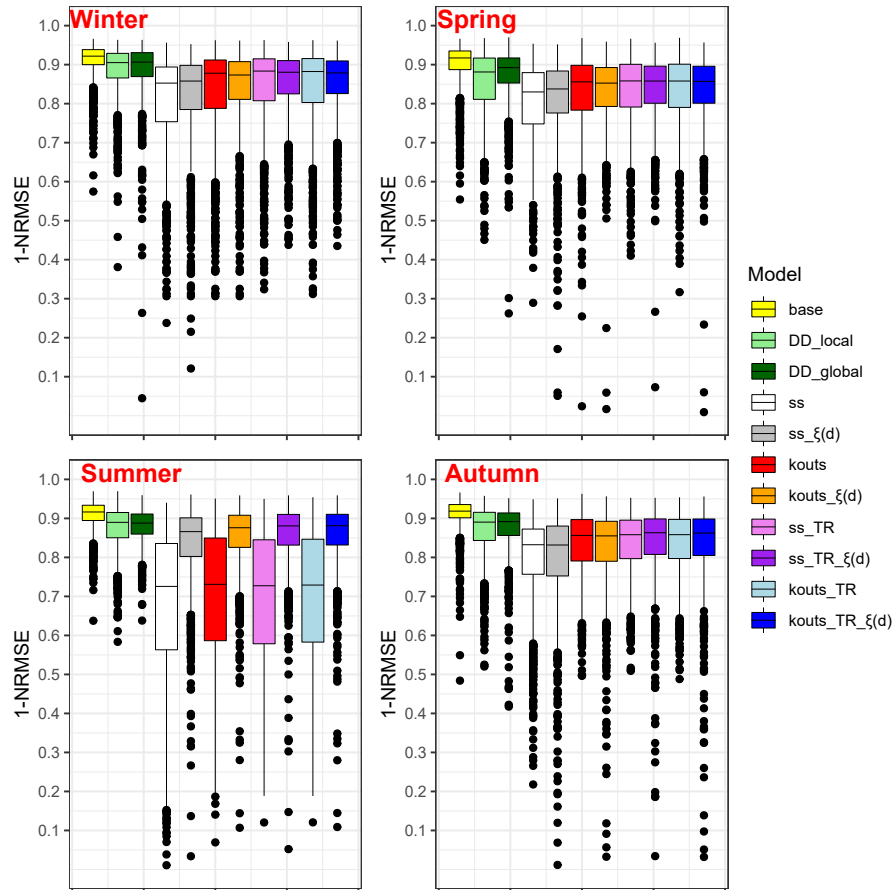


Figure 5. Boxplots of the (1-NRMSE) in calibration. Each boxplot contains 1053 points, each point corresponding to one station and duration.

431

4.2.2 Evaluation in cross-validation

432

433

434

435

436

The split-sampling procedure allows for the comparison of the models in a cross-validation framework. We use three regional criteria: NRMSE_{CV}, FF, and SPAN (see Section 3.4.2), to enable the comparison of the models based on their predictive capabilities. We want to select a model, which in addition to being able to fit the data used to train it, is able to perform reliably and robustly in the presence of new data.

437

438

439

440

441

442

In the following, we present the results in three paragraphs, first according to the reliability/accuracy of the model in predicting all the observations as measured by NRMSE_{CV}, then the reliability in predicting the maxima as measured by the FF criterion, and lastly, the robustness of the model in predicting the 100-year return level as measured by SPAN100. Figure 6 presents the results for the four seasons. For all the criteria, the model with a regional score equal to 1 is the best model.

443

444

445

446

447

For all seasons, the NRMSE_{CV} shows the data-driven models, specifically the IDF_{DD_{global}}, to be the most accurate/reliable in predicting the entire observations compared to the other models. In winter, however, the difference in the performance of the models is not very clear. Looking at the summer results, the models without accounting for $\xi = f(d)$ always have the worst performance.

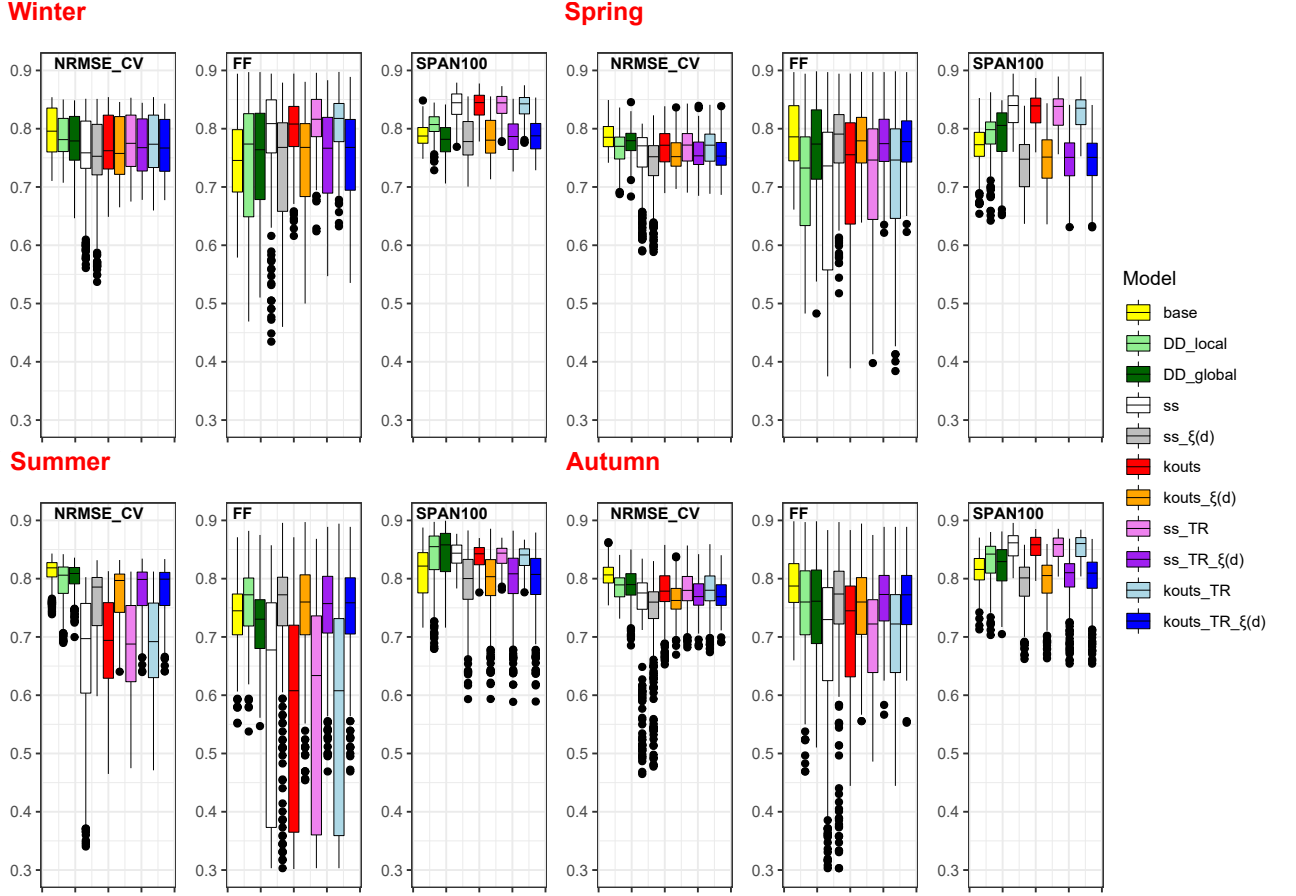


Figure 6. Boxplots of the regional cross-validation criteria, NRMSE_CV, FF, and SPAN. For the first two criteria, each boxplot contains 2×130 points, corresponding to one regional score for each of the 13 durations and 10 repetitions of the split-sampling. For the SPAN, each boxplot contains 130 points. The optimal value for each criterion is equal to 1.

448 In terms of the FF criterion, the best performance in predicting the maxima in winter
 449 is shown by the IDF_{ss_TR} model. In fact, all the models with no allowance for $\xi =$
 450 $f(d)$ happens to be the most reliable models in this season. The converse is however true
 451 in the case of the remaining seasons. In summer, while IDF_{DD_local} , is the best model,
 452 $IDF_{ss-\xi(d)}$ is the best in spring and autumn.

453 The robustness criteria, SPAN100 shows the models with no allowance for $\xi = f(d)$
 454 to be the most robust models. An exception to this is in summer, where the IDF_{DD_global}
 455 model is the most robust model. Also, higher robustness is found for the models not ac-
 456 counting for $\xi = f(d)$ compared to their counterparts, for example IDF_{ss} vs $IDF_{ss-\xi(d)}$.
 457 This is despite the fact that the former performs poorly in calibration, and is the least
 458 performing according to the other cross-validation criteria of reliability. This confirms
 459 the previous comments of Garavaglia et al. (2011) that a robust model can completely
 460 fail to model/predict the data. Hence the robustness criteria should only be used along-
 461 side other reliability criteria, such that the most robust model is only selected among
 462 models of similar reliability.

463 To summarize the results, the best IDF model should perform well in calibration,
 464 and should not be very sensitive to the data used to train it. In calibration, the data-

465 driven model $\text{IDF}_{DD_{global}}$ showed the best performance compared to all the other nine
 466 models, it also remain accurate and reliable at predicting the entire observations in the
 467 split-sampling cross-validation (as measured by the NRMSE.CV), especially in summer.
 468 This is an important feature since we are interested in the complete range of intensities.
 469 Finally, it generally showed more robustness compared to the other models of similar re-
 470 liability.

471 4.3 IDF curves

472 Figure 7a shows the IDF curves from two models, IDF_{ss} and $\text{IDF}_{DD_{global}}$, in sum-
 473 mer, at a station in Zurich which is located in the Northeast of Switzerland. In this re-
 474 gion, summer is the main season of heavy rainfall. As a reminder, the IDF_{ss} allows scal-
 475 ing only in the scale parameter, σ of the EGPD, the other two parameters (κ and ξ), are
 476 independent of duration. The $\text{IDF}_{DD_{global}}$ on the other hand allows each of the three pa-
 477 rameters to vary with duration. The curves are for return periods $T = 2, 5, 10, 40,$ and
 478 100 years, while points are the empirical levels for $T = 2, 5,$ and 10 years.

479 The IDF_{ss} performed poorly at predicting the empirical quantiles. The curves mod-
 480 eled by the $\text{IDF}_{DD_{global}}$ on the other hand are in agreement with the empirical levels.

481 Similar IDF curves for autumn are shown in Fig. 7b for a station in Locarno which
 482 is located in the Ticino area in the south of Switzerland. The Ticino area is subject to
 483 the heaviest precipitation compared to the other regions in Switzerland. Again, the $\text{IDF}_{DD_{global}}$
 484 was able to model empirical levels correctly both for the small and long durations.

485 In Fig. 7, the curves of the simple-scaling model (IDF_{ss}) are not parallel. This be-
 486 havior resulted from the definition of IDF models for non-zero precipitation in Eq. 4. From
 487 this equation, we see that the T -year return level is defined as $(1 - \frac{1}{T \times \delta_d})$. The term
 488 δ_d , representing the average number of non-zero precipitation varies across the durations
 489 leading to a non-constant slope for the different curves.

490 We finally show, in Fig 8 and 9 respectively, the seasonal 100-year return level maps
 491 for $d = 1\text{hr}$ and 24h. The levels were obtained with the best performing model, *i.e.* $\text{IDF}_{DD_{global}}$.
 492 Looking at the return levels for $d = 1\text{hr}$ (Fig. 8), we see that the levels in winter are
 493 the lowest, with no specific spatial pattern or variability. In spring, the levels in the north
 494 and Ticino starts to increase. Summer has the highest levels, and similar levels are ob-
 495 tained all along the northern plateau. In autumn, while the levels in the north are com-
 496 parable to those in winter, those in Ticino are comparable to those in summer. A dif-
 497 ferent spatial pattern is however observed for the 100-year return level at $d = 24\text{hr}$. Specif-
 498 ically for summer, the levels in the plateau are lower than those along the north regime.
 499 The exhibited spatial pattern of the levels produced by this model is similar to those ob-
 500 served in earlier studies (see Fukutome et al. (2015) for the hourly, and Haruna et al.
 501 (2022) for the 24hr precipitation).

502 4.4 Discussion

503 In the following paragraphs, we briefly discuss some of our choices in terms of the
 504 functional forms of the data-driven models, taking into account the varying shape pa-
 505 rameter with duration, and the issue of correlation in the data.

506 First, for the the data-driven models, we limited our choice of the functional re-
 507 lationships to simple parametric models, specifically to piece-wise linear models. Other
 508 choices would be possible such as smooth regression splines (e.g. Youngman, 2019, 2020).
 509 This choice has its advantage and drawback. The advantage is that the splines are able
 510 to automatically adjust to fit any form of relationship. The main drawback is that it is
 511 inherently non-parametric, and so the mapping of the IDF models, to allow predictions
 512 at ungauged locations, is not directly possible. One can only map the three EGPD pa-

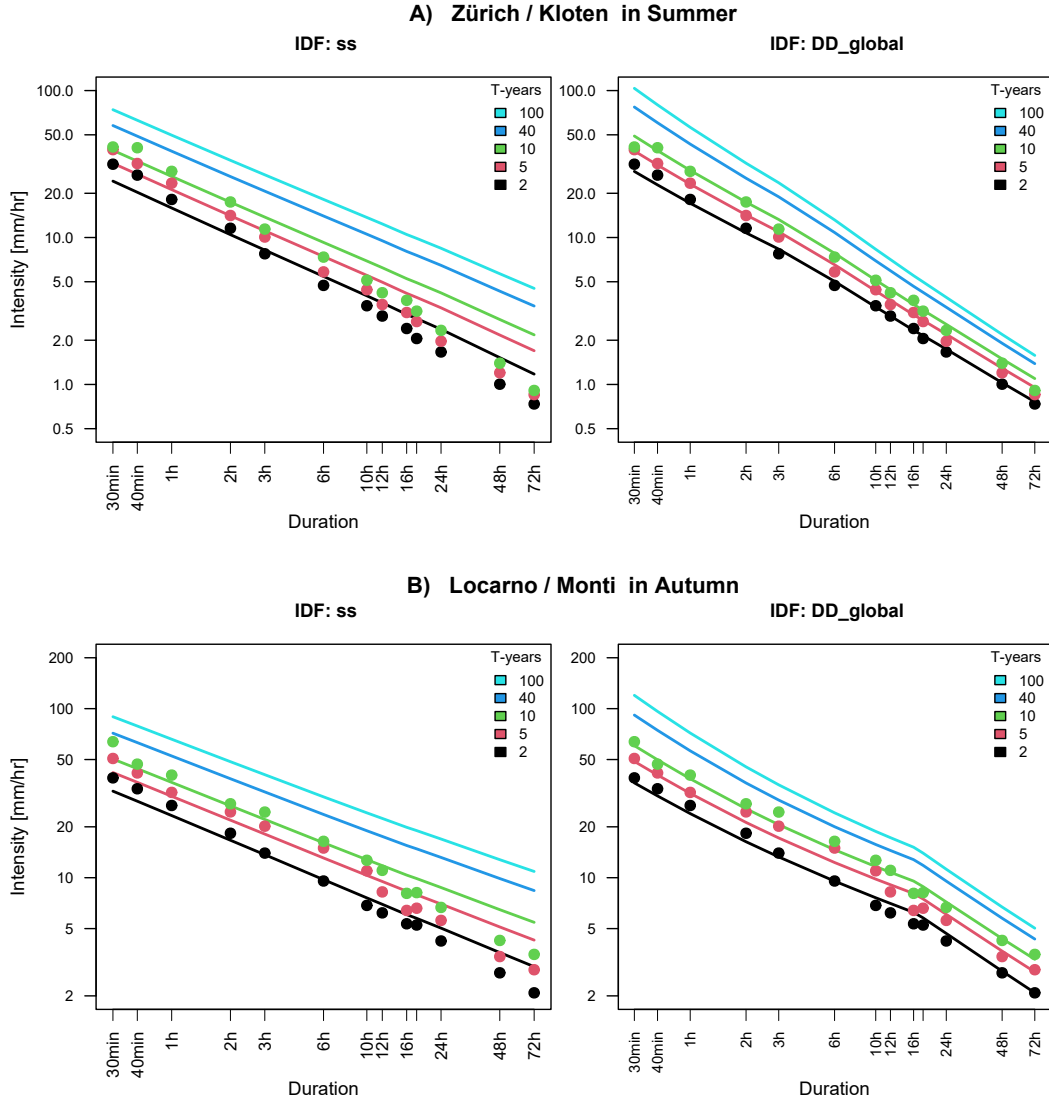


Figure 7. Simple-scaling (IDF_{ss}) and data-driven ($IDF_{DD_{global}}$) curves **a)** in summer at a station in Zurich (North-east). **b)** in autumn at a station in Locarno (Ticino area in the south). The curves are for the return periods $T = 2, 5, 10, 40$ and 100 years. The points are the empirical quantiles corresponding to $T = 2, 5$ and 10 years

513 rameters for a particular duration. For instance, for 13 durations, this means $3 \times 13 =$
 514 39 maps. For our choice of linear functions, 10 parameters are able to describe the IDF
 515 curves at each station, and hence 10 maps for the whole area under study.

516 Regarding the variation of the shape parameter ξ with respect to duration d , some
 517 earlier studies did observed or discussed it *e.g.* Veneziano et al. (2007) and Fauer et al.
 518 (2021). They however did not model it, either due to the weak form of the relationship,
 519 or because the IDF model did not allow for it. Here, especially, in summer, we found very
 520 strong dependence, and the results have shown that taking it into account is invaluable.

521 Finally it should be mentioned that throughout this work, we estimated the IDF
 522 models through the independence likelihood, thus omitting the correlation between dif-

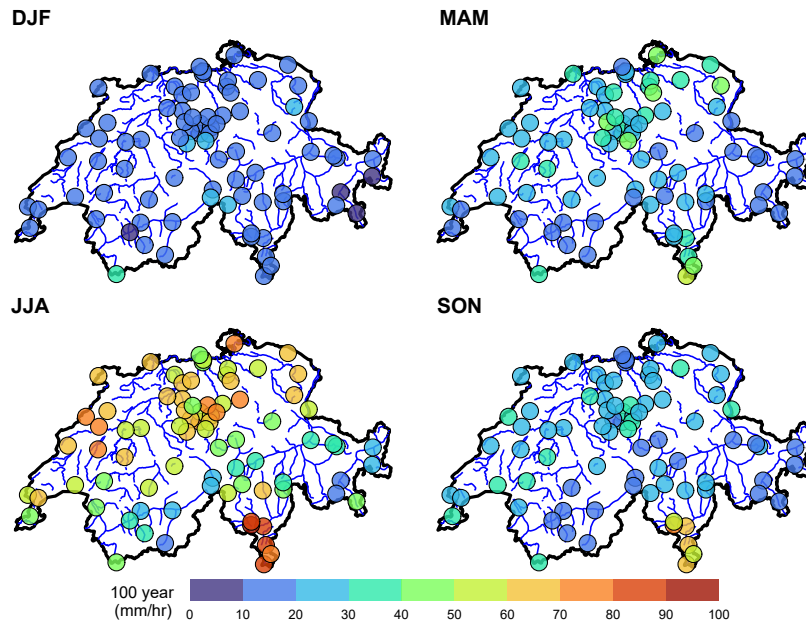


Figure 8. Map of Switzerland showing the seasonal 100-year return level in mm/hr for $d = 1$ hr. Levels predicted with $IDF_{DD_{global}}$.

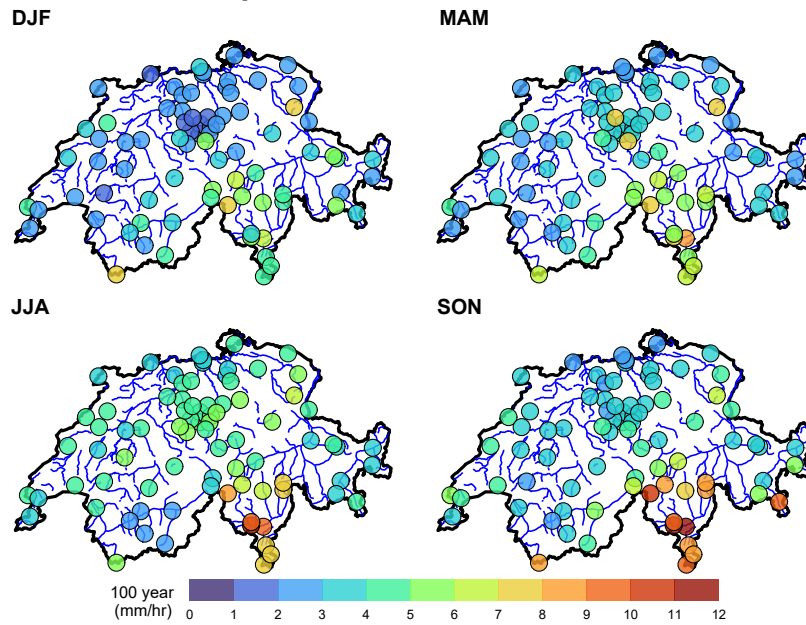


Figure 9. Map of Switzerland showing the seasonal 100-year return level in mm/hr for $d = 24$ hr. Levels predicted with $IDF_{DD_{global}}$.

523 ferent times and durations. Nadarajah et al. (1998) has modeled this using multivari-
 524 ate extreme value distributions (MEVD), and Tyrakis and Langousis (2019) followed suit
 525 by using max-stable processes. Later, Jurado et al. (2020), investigated the impact of
 526 accounting for the dependence in extremes and showed that there is little gain in per-
 527 formance, in addition to the added complexity of using max-stable processes.

528 5 Conclusions

529 Our aim in this paper was to build IDF curves using all the non-zero precipitation
 530 data in Switzerland. To achieve this, we used the EGPD model as the parametric model
 531 for the precipitation intensities. The literature presents various approaches to link the
 532 different durations together in IDF curves. We considered three of these approaches to
 533 build the IDF curves while using the EGPD as the parametric model. The first is the
 534 data-driven approach, where each parameter can vary with duration. The form of the
 535 relationship is fully determined by the data at hand. The second approach is based on
 536 the scale invariance theory, here IDF curves are built based on the scaling behavior of
 537 precipitation. The last approach is based on the general IDF formulation of Koutsoyiannis
 538 et al. (1998), which generalizes the various traditional IDF formulations.

539 We started from these three approaches and added some extensions to account for
 540 scaling break and varying shape parameter. We ended up with a total of ten IDF mod-
 541 els. We then compared them, first in calibration, and then in a split-sample cross-validation
 542 approach.

543 The results showed that, given the EGPD as the parametric model, the data-driven
 544 IDF-EGPD, particularly the $IDF_{DD_{global}}$, is the best model for the data at hand. This
 545 is despite being less parsimonious in terms of its number of free parameters. The IDF
 546 curves based on simple-scaling and the general formulation of Koutsoyiannis et al. (1998),
 547 did not perform as efficiently even with the added extensions in terms of scaling break
 548 and in the way the shape parameter varies with duration. The fact that the simple-scaling
 549 IDF models performed poorly in summer confirms the previous findings of Molnar and
 550 Burlando (2008) and (Paschalis, 2013) that in Switzerland, precipitation in summer shows
 551 multiscaling behavior.

552 In terms of perspectives, it would be interesting to produce maps of the paramete-
 553 rs to allow for predictions at ungauged sites. This could be achieved by simple inter-
 554 polation of the local IDF parameters as done by Blanchet et al. (2016), or through quan-
 555 tile regression methods (Ouali & Cannon, 2018), or by global estimation using spatial
 556 covariates (e.g. Ulrich et al., 2020). Another possibility is to use a regionalization tech-
 557 nique, such as the method of Hosking and Wallis (2005) and then interpolate the index
 558 flood to allow predictions at the ungauged sites (e.g. Mascaro, 2020).

559 Lastly, consideration of the effect of climate change in building IDF curves is in-
 560 valuable. For instance, Cheng and AghaKouchak (2014) showed that by neglecting non-
 561 stationarity in modeling IDF curves, there could be up to 60% underestimation of ex-
 562 treme precipitation, especially for short durations. It would therefore be interesting to
 563 model the curves while accounting for a warmer climate (e.g. Mirhosseini et al., 2013;
 564 Cheng & AghaKouchak, 2014; Ragno et al., 2018; Ouarda et al., 2019; Kristvik et al.,
 565 2019).

566 6 Open Research

567 The data used in this study are maintained by Swiss Federal Office of Meteorol-
 568 ogy and Climatology, MeteoSwiss (MeteoSwiss, 2021). It is available upon request at
 569 <https://gate.meteoswiss.ch/idaweb/> (last accessed 10 December 2021).

570 **Acknowledgments**

571 This research has been supported by the Bundesamt für Energie (grant no. SI/502150-
572 01) and the Bundesamt für Umwelt (grant no. SI/502150-01), through the *Extreme floods*
573 *in Switzerland* project.

574 **References**

- 575 Agbazo, M. N., Koto N’Gobi, G., Kounouhewa, B., Alamou, E., Afouda, A., &
576 Akpo, A. (2016, April). Estimation of IDF Curves of Extreme Rainfall by
577 Simple Scaling in Northern Oueme Valley, Benin Republic (West Africa).
578 *Earth Sciences Research Journal*, 20(1), 1–7. Retrieved 2021-09-09, from
579 <http://revistas.unal.edu.co/index.php/esrj/article/view/49405> doi:
580 10.15446/esrj.v20n1.49405
- 581 Ben-Zvi, A. (2009). Rainfall intensity–duration–frequency relationships derived from
582 large partial duration series. *Journal of Hydrology*, 367(1-2), 104–114. doi:
583 <https://doi.org/10.1016/j.jhydrol.2009.01.007>
- 584 Bernard, M. M. (1932). Formulas for rainfall intensities of long duration. *Trans-*
585 *actions of the American Society of Civil Engineers*, 96(1), 592–606. (Pub-
586 lisher: American Society of Civil Engineers) doi: <https://doi.org/10.1061/taceat.0004323>
- 587
- 588 Blanchet, J., Ceresetti, D., Molinié, G., & Creutin, J.-D. (2016, September). A re-
589 gional GEV scale-invariant framework for Intensity–Duration–Frequency analy-
590 sis. *Journal of Hydrology*, 540, 82–95. doi: 10.1016/j.jhydrol.2016.06.007
- 591 Blanchet, J., Paquet, E., Vaittinada Ayar, P., & Penot, D. (2019, February). Map-
592 ping rainfall hazard based on rain gauge data: an objective cross-validation
593 framework for model selection. *Hydrology and Earth System Sciences*, 23(2),
594 829–849. doi: 10.5194/hess-23-829-2019
- 595 Blanchet, J., Touati, J., Lawrence, D., Garavaglia, F., & Paquet, E. (2015). Eval-
596 uation of a compound distribution based on weather pattern subsampling
597 for extreme rainfall in Norway. *Nat. Hazards Earth Syst. Sci.*, 15. doi:
598 <https://doi.org/10.5194/nhess-15-2653-2015>
- 599 Bougadis, J., & Adamowski, K. (2006, November). Scaling model of a rainfall
600 intensity-duration-frequency relationship. *Hydrological Processes*, 20(17),
601 3747–3757. Retrieved 2021-09-06, from [https://onlinelibrary.wiley.com/](https://onlinelibrary.wiley.com/doi/10.1002/hyp.6386)
602 [doi/10.1002/hyp.6386](https://onlinelibrary.wiley.com/doi/10.1002/hyp.6386) doi: 10.1002/hyp.6386
- 603 Burlando, P., & Rosso, R. (1996, December). Scaling and multiscaling mod-
604 els of depth-duration-frequency curves for storm precipitation. *Jour-*
605 *nal of Hydrology*, 187(1), 45–64. Retrieved 2021-09-08, from [https://](https://www.sciencedirect.com/science/article/pii/S0022169496030867)
606 www.sciencedirect.com/science/article/pii/S0022169496030867 doi:
607 10.1016/S0022-1694(96)03086-7
- 608 Carreteras, M. T. (1987). Cálculo hidrometeorológico de caudales máximos en
609 pequeñas cuencas naturales. *Textos de la Direccion General de Carreteras*(12),
610 1987.
- 611 Chang, K. B., Lai, S. H., & Othman, F. (2016). Comparison of annual maxi-
612 mum and partial duration series for derivation of rainfall intensity-duration-
613 frequency relationships in peninsular malaysia. *Journal of Hydrologic Engi-*
614 *neering*, 21(1), 05015013. doi: 10.1061/(ASCE)HE.1943-5584.0001262
- 615 Cheng, L., & AghaKouchak, A. (2014). Nonstationary precipitation intensity-
616 duration-frequency curves for infrastructure design in a changing climate.
617 *Scientific reports*, 4(1), 1–6. doi: <https://doi.org/10.1038/srep07093>
- 618 Chow, V. (1962). Hydrologic determination of waterway areas for drainage struc-
619 tures in small drainage basins, Engrg. *Experimental Station, Univ. of Illinois,*
620 *Urbana I*, 11.
- 621 Courty, L. G., Wilby, R. L., Hillier, J. K., & Slater, L. J. (2019, August). Intensity-
622 duration-frequency curves at the global scale. *Environmental Research Letters*,

- 623 14(8), 084045. Retrieved 2022-01-18, from <https://doi.org/10.1088/1748>
 624 -9326/ab370a (Publisher: IOP Publishing) doi: 10.1088/1748-9326/ab370a
- 625 Evin, G., Blanchet, J., Paquet, E., Garavaglia, F., & Penot, D. (2016, October).
 626 A regional model for extreme rainfall based on weather patterns subsam-
 627 pling. *Journal of Hydrology*, 541, 1185–1198. Retrieved 2021-08-25, from
 628 <https://linkinghub.elsevier.com/retrieve/pii/S0022169416305145>
 629 doi: 10.1016/j.jhydrol.2016.08.024
- 630 Evin, G., Favre, A.-C., & Hingray, B. (2018). Stochastic generation of multi-site
 631 daily precipitation focusing on extreme events. *Hydrol. Earth Syst. Sci.*, 18.
 632 doi: <https://doi.org/10.5194/hess-22-655-2018>
- 633 Fauer, F. S., Ulrich, J., Jurado, O. E., & Rust, H. W. (2021, July). *Flexible and*
 634 *Consistent Quantile Estimation for Intensity-Duration-Frequency Curves*
 635 (preprint). Hydrometeorology/Modelling approaches. Retrieved 2021-11-26,
 636 from <https://hess.copernicus.org/preprints/hess-2021-334/> doi:
 637 10.5194/hess-2021-334
- 638 Fukutome, S., Liniger, M. A., & Süveges, M. (2015, May). Automatic threshold
 639 and run parameter selection: a climatology for extreme hourly precipita-
 640 tion in Switzerland. *Theoretical and Applied Climatology*, 120(3-4), 403–
 641 416. Retrieved 2021-04-19, from <http://link.springer.com/10.1007/s00704-014-1180-5> doi: 10.1007/s00704-014-1180-5
- 642 Garavaglia, F., Lang, M., Paquet, E., Gailhard, J., Garçon, R., & Renard, B.
 643 (2011). Reliability and robustness of rainfall compound distribution model
 644 based on weather pattern sub-sampling. *Hydrol. Earth Syst. Sci.*, 15. doi:
 645 <https://doi.org/10.5194/hess-15-519-2011>
- 646 Ghanmi, H., Bargaoui, Z., & Mallet, C. (2016). Estimation of intensity-duration-
 647 frequency relationships according to the property of scale invariance and re-
 648 gionalization analysis in a mediterranean coastal area. *Journal of Hydrology*,
 649 541, 38–49. doi: 10.1016/j.jhydrol.2016.07.002
- 650 Gupta, V. K., & Waymire, E. (1990). Multiscaling properties of spatial rainfall
 651 and river flow distributions. *Journal of Geophysical Research: Atmospheres*,
 652 95(D3), 1999–2009. doi: 10.1029/JD095iD03p01999
- 653 Gupta, V. K., & Waymire, E. C. (1993, February). A Statistical Analysis of
 654 Mesoscale Rainfall as a Random Cascade. *Journal of Applied Meteorology*
 655 *and Climatology*, 32(2), 251–267. doi: 10.1175/1520-0450(1993)032<0251:
 656 ASAOMR>2.0.CO;2
- 657 Harris, D., Seed, A., Menabde, M., & Austin, G. (1997, September). Factors af-
 658 fecting multiscaling analysis of rainfall time series. *Nonlinear Processes in Geo-*
 659 *physics*, 4(3), 137–156. Retrieved 2021-11-15, from [https://npg.copernicus](https://npg.copernicus.org/articles/4/137/1997/)
 660 [.org/articles/4/137/1997/](https://npg.copernicus.org/articles/4/137/1997/) doi: 10.5194/npg-4-137-1997
- 661 Haruna, A., Blanchet, J., & Favre, A.-C. (2022). Performance-based compari-
 662 son of regionalization methods to improve the at-site estimates of daily pre-
 663 cipitation. *Hydrology and Earth System Sciences*, 26(10), 2797–2811. doi:
 664 <https://doi.org/10.5194/hess-26-2797-2022>
- 665 Hosking, J. R. M., & Wallis, J. R. (2005). *Regional frequency analysis: an approach*
 666 *based on L-moments*. Cambridge ; New York: Cambridge University Press.
- 667 Innocenti, S., Mailhot, A., & Frigon, A. (2017, November). Simple scaling
 668 of extreme precipitation in North America. *Hydrology and Earth Sys-*
 669 *tem Sciences*, 21(11), 5823–5846. Retrieved 2021-09-08, from [https://](https://hess.copernicus.org/articles/21/5823/2017/)
 670 hess.copernicus.org/articles/21/5823/2017/ (Publisher: Copernicus
 671 GmbH) doi: 10.5194/hess-21-5823-2017
- 672 Jurado, O. E., Ulrich, J., Scheibel, M., & Rust, H. W. (2020, December). Eval-
 673 uating the Performance of a Max-Stable Process for Estimating Intensity-
 674 Duration-Frequency Curves. *Water*, 12(12), 3314. Retrieved 2022-01-27, from
 675 <https://www.mdpi.com/2073-4441/12/12/3314> (Number: 12 Publisher:
 676 Multidisciplinary Digital Publishing Institute) doi: 10.3390/w12123314

- 678 Katz, R. W., Parlange, M. B., & Naveau, P. (2002, August). Statistics of ex-
679 tremes in hydrology. *Advances in Water Resources*, *25*(8-12), 1287–1304.
680 Retrieved 2021-07-26, from [https://linkinghub.elsevier.com/retrieve/
681 pii/S0309170802000568](https://linkinghub.elsevier.com/retrieve/pii/S0309170802000568) doi: 10.1016/S0309-1708(02)00056-8
- 682 Koutsoyiannis, D., Kozonis, D., & Manetas, A. (1998, April). A mathemati-
683 cal framework for studying rainfall intensity-duration-frequency relation-
684 ships. *Journal of Hydrology*, *206*(1-2), 118–135. Retrieved 2021-09-06, from
685 <https://linkinghub.elsevier.com/retrieve/pii/S0022169498000973>
686 doi: 10.1016/S0022-1694(98)00097-3
- 687 Kristvik, E., Johannessen, B. G., & Muthanna, T. M. (2019). Temporal downscaling
688 of idf curves applied to future performance of local stormwater measures. *Sus-
689 tainability*, *11*(5), 1231. doi: <https://doi.org/10.3390/su11051231>
- 690 Langousis, A., & Veneziano, D. (2007, February). Intensity-duration-frequency
691 curves from scaling representations of rainfall. *Water Resources Research*,
692 *43*(2). Retrieved 2021-09-17, from [https://agupubs.onlinelibrary.wiley
693 .com/doi/10.1029/2006WR005245](https://agupubs.onlinelibrary.wiley.com/doi/10.1029/2006WR005245) (Publisher: John Wiley & Sons, Ltd) doi:
694 10.1029/2006WR005245
- 695 Le Gall, P., Favre, A.-C., Naveau, P., & Prieur, C. (2022). Improved regional fre-
696 quency analysis of rainfall data. *Weather and Climate Extremes*, *36*, 100456.
697 doi: <https://doi.org/10.1016/j.wace.2022.100456>
- 698 Lima, M. I. P. d. (1998). *Multifractals and the temporal structure of rainfall* (PhD
699 Thesis). Wageningen Agricultural University, Wageningen, Netherlands.
- 700 Madsen, H., Rosbjerg, D., & Harremoës, P. (1995, March). Application of the
701 Bayesian approach in regional analysis of extreme rainfalls. *Stochastic Hy-
702 drology and Hydraulics*, *9*(1), 77–88. Retrieved 2021-07-09, from [http://
703 link.springer.com/10.1007/BF01581759](http://link.springer.com/10.1007/BF01581759) doi: 10.1007/BF01581759
- 704 Mascaro, G. (2020). Comparison of local, regional, and scaling models for rainfall
705 intensity–duration–frequency analysis. *Journal of applied meteorology and cli-
706 matology*, *59*(9), 1519–1536. doi: <https://doi.org/10.1175/jamc-d-20-0094.1>
- 707 Menabde, M., Seed, A., & Pegram, G. (1999, January). A simple scaling model for
708 extreme rainfall. *Water Resources Research*, *35*(1), 335–339. Retrieved 2021-
709 09-17, from <http://doi.wiley.com/10.1029/1998WR900012> doi: 10.1029/
710 1998WR900012
- 711 MeteoSwiss. (2021). *Meteoswiss, federal office of meteorology and climatology*. Re-
712 trieved 2021-12-10, from <https://gate.meteoswiss.ch/idaweb/login.do>
- 713 Meylan, P., Favre, A.-C., & Musy, A. (2012). *Predictive hydrology: a frequency anal-
714 ysis approach*. CRC Press.
- 715 Mirhosseini, G., Srivastava, P., & Stefanova, L. (2013). The impact of climate
716 change on rainfall intensity–duration–frequency (idf) curves in alabama. *Re-
717 gional Environmental Change*, *13*(1), 25–33. doi: [https://doi.org/10.1007/
718 s10113-012-0375-5](https://doi.org/10.1007/s10113-012-0375-5)
- 719 Molnar, P., & Burlando, P. (2008). Variability in the scale properties of high-
720 resolution precipitation data in the Alpine climate of Switzerland. *Water Re-
721 sources Research*, *44*(10). doi: <http://doi.wiley.com/10.1029/2007WR006142>
- 722 Muggeo, V. M. (2003). Estimating regression models with unknown break-points.
723 *Statistics in medicine*, *22*(19), 3055–3071. doi: [https://doi.org/10.1002/
724 sim.1545](https://doi.org/10.1002/sim.1545)
- 725 Muggeo, V. M., et al. (2008). Segmented: an r package to fit regression models with
726 broken-line relationships. *R news*, *8*(1), 20–25.
- 727 Mèlèse, V., Blanchet, J., & Molinié, G. (2018, March). Uncertainty estima-
728 tion of Intensity–Duration–Frequency relationships: A regional analy-
729 sis. *Journal of Hydrology*, *558*, 579–591. Retrieved 2022-02-15, from
730 <https://linkinghub.elsevier.com/retrieve/pii/S002216941730519X>
731 doi: 10.1016/j.jhydrol.2017.07.054
- 732 Nadarajah, S., Anderson, C., & Tawn, J. (1998). Ordered multivariate extremes.

- 733 *Journal of the Royal Statistical Society: Series B (Statistical Methodology)*,
734 60(2), 473–496. doi: <https://doi.org/10.1111/1467-9868.00136>
- 735 Naveau, P., Huser, R., Ribereau, P., & Hannart, A. (2016, April). Model-
736 ing jointly low, moderate, and heavy rainfall intensities without a thresh-
737 old selection. *Water Resources Research*, 52(4), 2753–2769. Retrieved
738 2021-08-25, from <http://doi.wiley.com/10.1002/2015WR018552> doi:
739 10.1002/2015WR018552
- 740 Nhat, L. M., Tachikawa, Y., Sayama, T., & Takara, K. (2008). Estimation of sub-
741 hourly and hourly idf curves using scaling properties of rainfall at gauged site
742 in asian pacific region. *Annual of Disaster Prevention Research Institute. B*,
743 51(B), 63–73. doi: <https://doi.org/10.1016/j.atmosres.2004.10.025>
- 744 Ouali, D., & Cannon, A. (2018). Estimation of rainfall intensity–duration–frequency
745 curves at ungauged locations using quantile regression methods. *Stochastic En-
746 vironmental Research and Risk Assessment*, 32(10), 2821–2836. doi: <https://doi.org/10.1007/s00477-018-1564-7>
- 747
- 748 Ouarda, T. B., Yousef, L. A., & Charron, C. (2019). Non-stationary intensity-
749 duration-frequency curves integrating information concerning teleconnections
750 and climate change. *International Journal of Climatology*, 39(4), 2306–2323.
751 doi: <https://doi.org/10.1002/joc.5953>
- 752 Over, T. M. (1995). *Modeling space-time rainfall at the mesoscale using random cas-
753 cades* (PhD Thesis). University of Colorado, Boulder.
- 754 Overeem, A., Buishand, A., & Holleman, I. (2008, January). Rainfall depth-
755 duration-frequency curves and their uncertainties. *Journal of Hydrol-
756 ogy*, 348(1-2), 124–134. Retrieved 2021-11-30, from [https://linkinghub
757 .elsevier.com/retrieve/pii/S0022169407005513](https://linkinghub.elsevier.com/retrieve/pii/S0022169407005513) doi: 10.1016/
758 j.jhydrol.2007.09.044
- 759 Panthou, G., Vischel, T., Lebel, T., Quantin, G., & Molinié, G. (2014, December).
760 Characterising the space–time structure of rainfall in the Sahel with a view to
761 estimating IDAF curves. *Hydrology and Earth System Sciences*, 18(12), 5093–
762 5107. Retrieved 2021-11-04, from [https://hess.copernicus.org/articles/
763 18/5093/2014/](https://hess.copernicus.org/articles/18/5093/2014/) doi: 10.5194/hess-18-5093-2014
- 764 Paschalis, A. (2013). *Modelling the Space-Time Structure of Precipitation and its
765 Impact on Basin Response* (Doctoral dissertation, ETH Zurich). doi: 10.3929/
766 ETHZ-A-009917135
- 767 Ragno, E., AghaKouchak, A., Love, C. A., Cheng, L., Vahedifard, F., & Lima, C. H.
768 (2018). Quantifying changes in future intensity-duration-frequency curves
769 using multimodel ensemble simulations. *Water Resources Research*, 54(3),
770 1751–1764. doi: <https://doi.org/10.1002/2017wr021975>
- 771 Renard, B., Kochanek, K., Lang, M., Garavaglia, F., Paquet, E., Neppel, L., ...
772 Auffray, A. (2013, February). Data-based comparison of frequency analysis
773 methods: A general framework. *Water Resources Research*, 49(2), 825–843.
774 Retrieved 2021-06-29, from [https://agupubs.onlinelibrary.wiley.com/
775 doi/10.1002/wrcr.20087](https://agupubs.onlinelibrary.wiley.com/doi/10.1002/wrcr.20087) doi: 10.1002/wrcr.20087
- 776 Ritschel, C., Ulbrich, U., Névir, P., & Rust, H. W. (2017). Precipitation extremes
777 on multiple timescales–bartlett–lewis rectangular pulse model and intensity–
778 duration–frequency curves. *Hydrology and Earth System Sciences*, 21(12),
779 6501–6517. doi: <https://doi.org/10.5194/hess-21-6501-2017>
- 780 Rivoire, P., Martius, O., & Naveau, P. (2021). A Comparison of Moderate and
781 Extreme ERA-5 Daily Precipitation With Two Observational Data Sets.
782 *Earth and Space Science*, 8(4), e2020EA001633. Retrieved 2022-03-22, from
783 <https://onlinelibrary.wiley.com/doi/abs/10.1029/2020EA001633> doi:
784 10.1029/2020EA001633
- 785 Roksvåg, T., Lutz, J., Grinde, L., Dyrddal, A. V., & Thorarinsdottir, T. L. (2021).
786 Consistent intensity-duration-frequency curves by post-processing of esti-
787 mated bayesian posterior quantiles. *Journal of Hydrology*, 603, 127000. doi:

- 788 <https://doi.org/10.1016/j.jhydrol.2021.127000>
- 789 Sane, Y., Panthou, G., Bodian, A., Vischel, T., Lebel, T., Dacosta, H., ...
- 790 Diop Kane, M. (2018, July). Intensity–duration–frequency (IDF) rainfall
- 791 curves in Senegal. *Natural Hazards and Earth System Sciences*, 18(7), 1849–
- 792 1866. (Publisher: Copernicus GmbH) doi: 10.5194/nhess-18-1849-2018
- 793 Schertzer, D., & Lovejoy, S. (1987). Physical Modeling and Analysis of Rain and
- 794 Clouds by Anisotropic Scaling Multiplicative Processes. *Journal of Geophysical*
- 795 *Research*, 92, 22. doi: <https://doi.org/10.1029/jd092id08p09693>
- 796 Sherman, C. W. (1931). Frequency and intensity of excessive rainfalls at Boston,
- 797 Massachusetts. *Transactions of the American Society of Civil Engineers*,
- 798 95(1), 951–960. (Publisher: American Society of Civil Engineers) doi:
- 799 <https://doi.org/10.1061/taceat.0004286>
- 800 Tencaliec, P., Favre, A., Naveau, P., Prieur, C., & Nicolet, G. (2020). Flexible semi-
- 801 parametric generalized Pareto modeling of the entire range of rainfall amount.
- 802 *Environmetrics*, 31(2). doi: 10.1002/env.2582
- 803 Tyralis, H., & Langousis, A. (2019, January). Estimation of inten-
- 804 sity–duration–frequency curves using max-stable processes. *Stochastic En-*
- 805 *vironmental Research and Risk Assessment*, 33(1), 239–252. Retrieved
- 806 2022-01-27, from <https://doi.org/10.1007/s00477-018-1577-2> doi:
- 807 10.1007/s00477-018-1577-2
- 808 Ulrich, J., Jurado, O. E., Peter, M., Scheibel, M., & Rust, H. W. (2020, November).
- 809 Estimating IDF Curves Consistently over Durations with Spatial Covariates.
- 810 *Water*, 12(11), 3119. Retrieved 2021-12-10, from [https://www.mdpi.com/](https://www.mdpi.com/2073-4441/12/11/3119)
- 811 [2073-4441/12/11/3119](https://www.mdpi.com/2073-4441/12/11/3119) doi: 10.3390/w12113119
- 812 Van de Vyver, H. (2018). A multiscaling-based intensity–duration–frequency model
- 813 for extreme precipitation. *Hydrological Processes*, 32(11), 1635–1647. (eprint:
- 814 <https://onlinelibrary.wiley.com/doi/pdf/10.1002/hyp.11516>) doi: 10.1002/hyp
- 815 .11516
- 816 Van de Vyver, H., & Demarée, G. R. (2010). Construction of Inten-
- 817 sity–Duration–Frequency (IDF) curves for precipitation at Lubumbashi,
- 818 Congo, under the hypothesis of inadequate data. *Hydrological Sciences Jour-*
- 819 *nal*, 55(4), 555–564. doi: 10.1080/02626661003747390
- 820 Veneziano, D., & Lepore, C. (2012). The scaling of temporal rainfall. *Water Re-*
- 821 *sources Research*, 48(8). doi: 10.1029/2012WR012105
- 822 Veneziano, D., Lepore, C., Langousis, A., & Furcolo, P. (2007, October). Marginal
- 823 methods of intensity-duration-frequency estimation in scaling and nonscaling
- 824 rainfall. *Water Resources Research*, 43(10). doi: 10.1029/2007WR006040
- 825 Willems, P. (2000). Compound intensity/duration/frequency-relationships of ex-
- 826 treme precipitation for two seasons and two storm types. *Journal of Hydrology*,
- 827 233(1), 189–205. doi: 10.1016/S0022-1694(00)00233-X
- 828 Youngman, B. D. (2019, October). Generalized Additive Models for Exceedances
- 829 of High Thresholds With an Application to Return Level Estimation for U.S.
- 830 Wind Gusts. *Journal of the American Statistical Association*, 114(528), 1865–
- 831 1879. Retrieved 2021-07-26, from [https://www.tandfonline.com/doi/full/](https://www.tandfonline.com/doi/full/10.1080/01621459.2018.1529596)
- 832 [10.1080/01621459.2018.1529596](https://www.tandfonline.com/doi/full/10.1080/01621459.2018.1529596) doi: 10.1080/01621459.2018.1529596
- 833 Youngman, B. D. (2020, November). evgam: An R package for Generalized Additive
- 834 Extreme Value Models. *arXiv:2003.04067 [stat]*. Retrieved 2021-04-19, from
- 835 <http://arxiv.org/abs/2003.04067> (arXiv: 2003.04067)
- 836 Yu, P.-S., Yang, T.-C., & Lin, C.-S. (2004, August). Regional rainfall intensity for-
- 837 mulas based on scaling property of rainfall. *Journal of Hydrology*, 295(1), 108–
- 838 123. Retrieved 2021-11-17, from [https://www.sciencedirect.com/science/](https://www.sciencedirect.com/science/article/pii/S0022169404001362)
- 839 [article/pii/S0022169404001362](https://www.sciencedirect.com/science/article/pii/S0022169404001362) doi: 10.1016/j.jhydrol.2004.03.003